Proc. Vth International Workshop, Advances in Signal Processing for Non Destructive Evaluation of Materials
Québec City (Canada),2-4 Aug. 2005. © X. Maldague ed., É. du CAO (2006), ISBN 2-9809199-0-X

Shape Effect on Blind Frequency for Depth Inversion in Pulsed Thermography

M. Genest[1], E. Grinzato[2], P. Bison[2], S. Marinetti[2]
C. Ibarra-Castanedo[1], X. Maldague[1]
[1] Electrical and Computing Eng. Dept., Université Laval, Quebec City (Quebec) Canada[1]
[2] ITC-CNR, Padova (Venice) Italy[2]

Abstract

In this paper, a study is presented indicating that the specimen shape, for orientation smaller than about 30°, does not affect the blind frequency obtained in Pulsed Phase Thermography processing. Therefore, it makes this measurement suitable for depth inversion in the case of non-flat shaped specimens. Theory and experimental results are discussed.

1. Introduction

Infrared (IR) pulsed thermography (PT) [1] experiences a fast deployment in NonDestructive (NDE) evaluation nowadays. In some instances, the part to be inspected is of complex shape. Little studies have been devoted to those cases, especially if quantitative depth retrieval is of interest (see for instance [2, 3, 4]). In fact it is easily conceived that, with respect to a situation where a specimen is flat, the case of a complex shape - let say a tilted for now – specimen will provide a different temperature measurement if all other parameters are the same. This is due to the local orientation θ of the surface (Fig. 1, left).

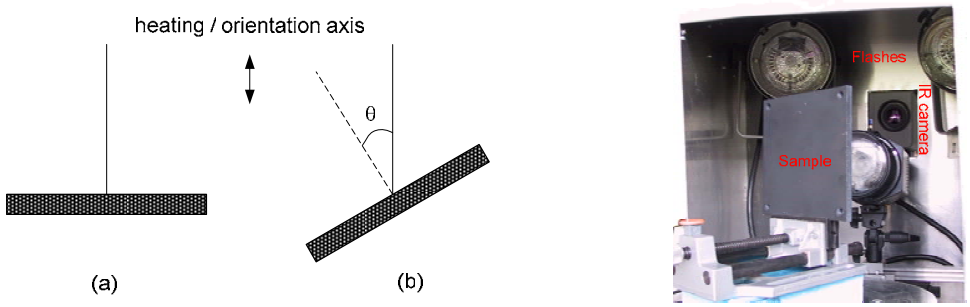

Figure 1 Flat and tilted plate (left), experimental set-up for IR thermography NDE (right).

We recall that in pulsed thermography, the specimen is submitted to a thermal pulse which causes its surface temperature to rise. Assuming a photo-thermal pulse of energy, the specimen surface temperature rises and then decays due to natural cooling (Fig. 1, right). The temperature decay is of interest since thermal waves launched into the specimen by the heating pulse reveal defects at a time which depends on defect depth [1].

[1] maldagx@gel.ulaval.ca
[2] ermanno.grinzato@itc.cnr.it, paolo.bison@itc.cnr.it, sergio.marinetti@itc.cnr.it

Pulsed Phase Thermography (PPT) is a signal processing in which the specimen behaviour in PT is analysed not in the time domain but rather in the frequency domain [4]. PPT studies were found particularly helpful if phase is considered. Moreover, recent studies showed that depth inversion can be easily performed by extracting blind frequencies [5]. In this paper, the effect of shape orientation (that is local orientation θ) is considered in regards of depth inversion with blind frequency.

2. Theory

2.1 On orientation θ

Pulsed heating of a semi-infinite homogeneous specimen (Fig. 1-a, left) causes the surface temperature to rise and then decay. Assuming a simple 1-D case, the temperature decay T can be defined as [1, eq. 9.8]:

$$T = \frac{Q}{e\sqrt{\pi t}} \tag{1}$$

where Q is the amount of energy absorbed by the specimen, t is the time and e is the thermal effusivity of the specimen defined as $\sqrt{k\rho C}$ with k the thermal conductivity, ρ the mass density and C the specific heat.

If we suppose a PPT subsequent processing [5], the temperature decay recorded by the IR camera (Fig. 1, right) will be subject to a discrete Fast Fourier Transform (FFT) so that data is moved from the time domain (discretized here as N data per image pixel along the time axis) to the frequency domain leading to:

$$T(k) \Leftrightarrow F(n) \tag{2}$$

$$F = \sum_{k=0}^{N-1} T(k) e^{2\pi i k n / N} = \mathrm{Re}_n + i\,\mathrm{Im}_n \tag{3}$$

where F is the FFT of T, i is the imaginary number ($\sqrt{-1}$), Re and Im are the real and imaginary parts of the transform, k stands for the time increment and the n designates the frequency increment.

The phase and amplitude images are finally obtained from the known relationships:

$$A_n = \sqrt{\mathrm{Re}_n^2 + \mathrm{Im}_n^2} \text{ and } \phi_n = \arctan\left(\frac{\mathrm{Im}_n}{\mathrm{Re}_n}\right). \tag{4}$$

Now, in the case of a tilted component and assuming a uniform surface heating Q of the surface, we have to consider the surface orientation θ. Angle θ affects the measurement in two ways. First, assuming orthographic heating, only cos θ of the energy contributes to the heating (this comes from the projection in the heating direction). Second for a "lambertian" surface, only cos θ of the subsequent surface heating will be emitted in the

direction of the IR camera (this comes from the projection in the observation direction). Hence, the observed tilted surface temperature T' will be reduced by a factor:

$$T' = \cos^2\theta \cdot T \,. \tag{5}$$

Following eq. (3), knowing that the Fourier transform is a linear operator, and since $\cos^2\theta$ is a constant here (it does not depend upon time), we see that:

$$A_n' \approx \sqrt{\cos^2\theta \cdot \mathrm{Re}_n^2 + \cos^2\theta \cdot \mathrm{Im}_n^2} \text{ and } \phi_n' \approx \arctan\left(\frac{\cos^2\theta \cdot \mathrm{Im}_n}{\cos^2\theta \cdot \mathrm{Re}_n}\right). \tag{6}$$

Here "≈" symbol was used since such an analysis is only approximative due to the particular irradiation deployed. Clearly, in PPT, amplitude A images will be affected by surface orientation θ while phase ϕ images should not be much since parameter $\cos^2\theta$ cancels out in the division process of eq. (6).

Before terminating this section, the following table shows the value of $\cos^2\theta$ for several orientation θ. It is seen than for orientations of less than about 30° surface orientation should not affect much the data assuming a common level of uncertainty (Table 1).

Table 1. Values of $\cos^2\theta$ as function of θ.

θ	$\cos^2\theta$	θ	$\cos^2\theta$
10°	0.97	40°	0.59
20°	0.88	50°	0.41
30°	0.75	60°	0.25

2.2 On depth inversion with blind frequency f_b

In PPT, the blind frequency f_b is the frequency at which the phase value ϕ_d of a defect of given depth z_d merges with the phase value of the sound material [7]. It was demonstrated that f_b and z_d can be related using the following relationship for depth inversion [6]:

$$z_d = C_1 \phi_d \sqrt{\frac{\alpha_d}{\pi f_b}} + C_2 \tag{7}$$

Where C_1 and C_2 are regression coefficients C_1 being related to material properties and α_d is the thermal diffusivity ($\alpha_d = k/\rho C$). This equation is directly derived after the thermal diffusion length $\mu_d = (\alpha_d / \pi f_b)^{1/2}$. In fact in [8], author mentions a value of $C_1 \approx 1.8$.

3. Experiments

In order to verify the previous discussion, several experiments where conducted on two different specimens, identical in all respect but *Specimen 1* was made of CFRP (Carbon Fiber Reinforced Plastic) while *Specimen 2* was made of GFRP (Glass Fiber Reinforced Plastic). Both samples have the shape of a cylinder with a curvature radius of 27.5 cm and several defects (square Teflon inserts of different sizes: 5 rows of 5 square defects of size: 3, 5, 7, 10, 15 mm and of different depths from 0.2 to 1 mm) located between plies during fabrication. Furthermore, during the experiments, the specimens were tilted with respect to the heating/observation axis (Fig. 1) to get more orientations to analyse (Fig. 2).

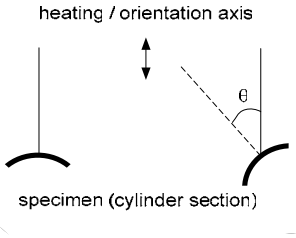

Fig. 2 Specimen tilted with various orientations θ.

The specimen was tested by pulsed thermography (Fig. 1, right). Figure 3 confirms what was said in Section 2 (eq. (6)): phase is relatively insensitive to orientation while amplitude is.

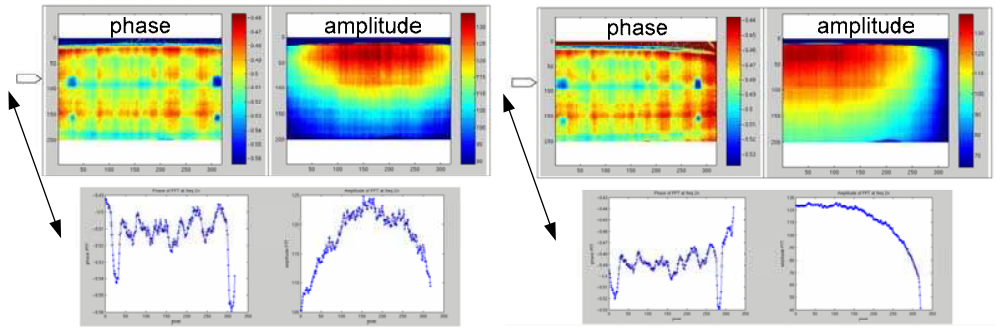

Fig. 3 Effect of orientation on phase and amplitude for *Specimen* 1 made of CFRP with orientation of (a): 0° and (b): 20°. Second discrete frequency (0.167 Hz).
Plots along image row are also shown.

Interestingly, a simple normalization of the temperature can remove most of the unwanted effects of shape variation (and uneven heating since uniform heating is hardly achieved). The normalization function consists in the division of each frame (k) of the temporal temperature T sequence by the first frame after the heating pulse. This can be expressed by the following equation (Fig. 4 shows some results):

$$T_{k\,normalized} = T_k / T_1 \qquad (8)$$

Following Section 2.2, blind frequencies were then extracted. Since data was subject to noise (as shown on the plots of Fig. 3 and 4), smoothing was performed by fitting the phase data with a logarithmic polynomial (as in temperature reconstruction [9]). Fig. 5 shows the phase for the five different defect depths of the specimen.

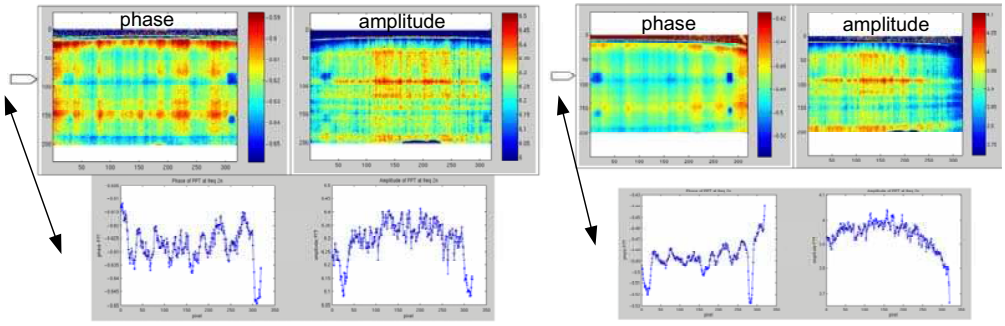

(a) (b)

Fig. 4 Effect of orientation on phase and amplitude for *Specimen* 1 with orientation of (a): 0° and (b): 20°. Second discrete frequency (0.167 Hz). Plots along image row are also shown. Phase and amplitude after normalization of temperature sequence.

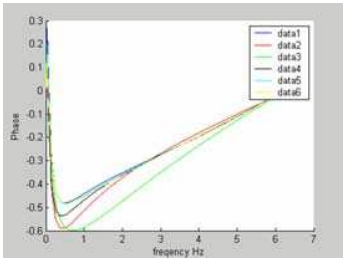

Fig. 5 Typical phase evolution from the shallowest to the deepest defect ranking (0.2 mm increment): 3, 2, 4, 5, 1 and data 6 is the selected reference area (non-defect). Results were obtained using 400 frames at an acquisition speed of 25 Hz, allowing a minimum frequency of 0.0625 Hz and maximum frequency of 12.5 Hz. Specimen orientation was 0°. *Specimen* 1.

Several tests were performed over defects of different sizes yielding to similar blind frequencies. In fact, provided the defect was large enough (size-on-depth ratio >> 1), size does not affect blind frequency (at least as long as the defect can be detected!). In the present study, size-on-depth ratio varies from 3 (minimum) to 75 (maximum). Table 2 summarizes the results for different depths with orientation 0°.

Table 2. Experimental average blind frequencies for different depths (here we refer to depths by specimen plies), *Specimen* 1.

Orientation: 0°	5^{th} and 6^{th} ply	4^{th} and 5^{th} ply	3^{rd} and 4^{th} ply	2^{nd} and 3^{rd} ply	1^{st} and 2^{nd} ply
blind frequency	0.75	1.2125	1.5	2.5875	7

The next step was to study the effect of orientation on blind frequency. Results are presented in Table 3.

Table 3. Experimental average blind frequencies for different depths and orientations. *Specimen* 1.

Orientation	5th and 6th ply	4th and 5th ply	3rd and 4th ply	2nd and 3rd ply	1st and 2nd ply
0°	0.689	0.75	1.13	2.38	6.81
10°	0.44	1.13	1.50	2.25	6.63
20°	0.44	2.19*	1.69	2.56	7.31
30°	0.63	1.13	1.57	2.44	6.94
40°	0.8125	-	1.8125	2.3750	8.00*
40° position 2	0.75	-	1.25	2.25	7.06
50°	1.06	-	1.75	2.38	7.13

* suspected data!

From Table 3, we notice the orientation does not affect significatively the blind frequency, at least if the orientation is reasonable ($\theta < 30°$, Table 1). In fact, if values of Table 3 are averaged (Table 4), we obtained similar values as listed in Table 2.

Table 4. Blind frequency for different depths (averaged values of Table 3). *Specimen* 1.

	5th and 6th ply	4th and 5th ply	3rd and 4th ply	2nd and 3rd ply	1st and 2nd ply
Mean	0.69	1.30	1.53	2.38	7.13*
std	0.2195	0.6195	0.2573	0.1083	0.4449*

* Removing the value of 8.00 at 40°, a mean of 6.98 and standard deviation of 0.2426 are obtained.

On Fig. 6 the evolution of blind frequency as function of depth is plotted after data of Table 4, such a curve can be used for calibration purpose (eq. 7).

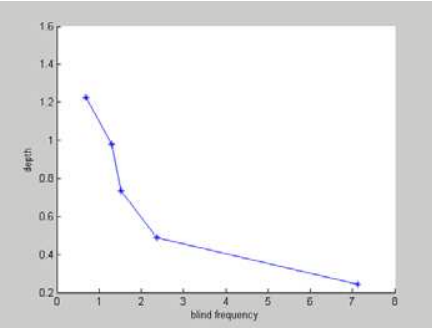

Fig. 6 Blind frequency for different depths. *Specimen* 1.

Specimen 2 (GFRP) was similarly tested without application of any paint. Since this material is partly transparent (in both visible and infrared spectra), mitigate results were obtained and a threshold had to be applied to the phase contrast (difference of phase between point of interest and reference area) due to the high noise level. The high noise level prevents the full analysis of defects at all depths. Nevertheless, results from the shallowest defect indicate orientation does not affect the blind frequency, at least for reasonable orientations ($\theta < 30°$, Table 1). Table 5 list the experimental frequencies as function of depth for the 0° orientation case.

Table 5 Averaged blind frequency for different depths with 0° orientation. *Specimen* 2.

Orientation: 0°	5^{th} and 6^{th} ply	4^{th} and 5^{th} ply	3^{rd} and 4^{th} ply	2^{nd} and 3^{rd} ply	1^{st} and 2^{nd} ply
Mean	0.39	0.97	1.83	2.46	5.57

4. Conclusion

In this paper, a study of the blind frequency as function of surface orientation was performed. We conclude that, for reasonable orientations ($\theta < 30°$), blind frequencies are not affected by orientation. Moreover, we noted blind frequencies are also size invariant provided that defect size-on-depth ratio is sufficiently high (>> 1). Results were obtained on both CFRP and GRFP. It is recommended to apply a coating on GFRP due to the semi-transparent nature of this material.

5. Acknowledgements

The support of Ministère des affaires étrangères du Québec and from Ministri Affari Esteri of Italy is acknowledged.

6. References

[1] Maldague X.P.V., Theory *and Practice of Infrared Technology for Non Destructive Testing*, John-Wiley & Sons, 684 p., 2001.
[2] X. Maldague, E. Barker, A. Nouah, E. Boisvert, B. Dufort, L. Fortin, "On methods for shape correction and reconstruction in thermographic NDT," *IInd Workshop on Advances in signal processing for NDE of Materials*, Kluwer Academic Pub., **E – 262:** 209-224, 1994.
[3] J.F.Pelletier, E. Grinzato, R. Dessì, X. Maldague: "Shape and uneven heating correction for NDT on cylinders by thermal methods", QIRT 96: 263-268, 1996..
[4] V.P.Vavilov, S.Marinetti: "Pulsed Phase Thermography and Fourier-Analysis Thermal Tomography", *Russian Journal of Nondestructive Testing*, **35:** 2, pp. 134-145, (from *Defectoscopyia* No.2, pp. 58-71, Russia), 1999.
[5] X. Maldague, S. Marinetti, "Pulse Phase Infrared Thermography," *J. Appl. Phys*, **79**(5): 2694-2698, 1996.
[6] C. Ibarra-Castanedo, N. P. Avdelidis, X. Maldague "Quantitative Pulsed Phase Thermography Applied to Steel Plates," *Thermosense XXVII*, **5782**: 342-352, 2005.

[7] Bai W., Won B. S. "Evaluation Defects in Composite Plates under Convective Environments using Lock-In Thermography," Meas. Sci. Technol.s **12**: 142-150, 2001.
[8] Busse G. "Optoacoustic Phase Angle Measurement for Probing a Metal," Appl. Phys. Lett., **36**(10): 815-816, 1979.
[9] Shepard S. M. "Advances in Pulsed Thermography," *Thermosense XXIII*, **4360**: 511-515, 2001.